Available online at www.sciencedirect.com
ScienceDirect
Journal of the European Ceramic Society 30 (2010) 1–10
www.elsevier.com/locate/jeurceramsoc

Solvent-based paste extrusion solid freeforming

Xuesong Lu [a], Yoonjae Lee [b], Shoufeng Yang [c], Yang Hao [b], Julian R.G. Evans [a,*], Clive G. Parini [b]

[a] Department of Chemistry, University College London, 20 Gordon Street, London WC1H 0AJ, UK
[b] Department of Electronic Engineering, Queen Mary, University of London, Mile End Road, London E1 4NS, UK
[c] Department of Materials, Queen Mary, University of London, Mile End Road, London E1 4NS, UK

Received 31 March 2009; received in revised form 20 June 2009; accepted 18 July 2009
Available online 21 August 2009

Abstract

Solvent-based extrusion freeforming is capable of building complex ceramic 3D structures and can be used in the fabrication of hard and soft tissue scaffolds, photonic crystals for millimetre wave, ordered ceramic preforms for metal matrix composites, precise molten metal filters and potentially for terahertz bandgap metamaterials. This is a powder-based rapid prototyping process, the principle of which is the realization of liquid to solid transition through solvent evaporation in the presence of a binder. We describe the characteristics of pastes prepared from different powders, notably the rheological properties at different solvent fractions and illustrate some of the structures fabricated by this technique.

Keywords: Extrusion; Freeforming; Drying; Al_2O_3; Functional application

1. Introduction

Solid freeforming can be defined as the creation of a shape by point, line or planar addition of material without confining surfaces other than a base. Paste extrusion freeforming (EFF)[1] along with fused deposition modelling (FDM),[2] direct-write assembly (DW),[3] micropen (MP)[4] and robocasting (RC)[5] are all in the group of linear methods in which a strand, filament or line is deposited. This enables the construction of complex 3D structures by building a layer or slice of the design file at a time. Thus immediate downloading of a 3D design without the need for expensive tooling or lithographic masks[6] is possible and can be used for fabrication of metamaterials[7,8] and tissue scaffolds[3,9] and many other devices.

Members of this family of processes each make use of a state change which can be solidification by crystallisation, liquid to glass transition, gelation, polymerisation, dilatant transition or solvent evaporation. During extrusion, the material is in a liquid state so that extrusion pressure is low and flow is facilitated. After extrusion, the material changes rapidly into the solid state so that 3D structures can be formed without sagging or other deformation defects. These techniques operate around the liquid-to-solid state transitional conditions. An example of temperature-dependent freeforming is fused deposition modelling (FDM)[10,11] which uses a thermoplastic polymer (e.g. ABS P400) to deposit a filament rapidly (typically in ~1 s) from the melt (270 °C) to the glass-transition temperature (94 °C). A typical gelation method is direct-writing assembly in which a soft or solid-like material with a liquid component[12] undergoes a liquid to gel transition. For example, control of colloidal forces to generate a highly concentrated stable dispersion is followed by inducing a state change through modifying pH, ionic strength or solvent quantity to promote a fluid-to-gel transition.[13] Various different suspensions for freeforming, such as polyvinyl-pyrrolidone (PVP) sol–gel ink,[14] polyelectrolyte ink[15] including poly(ethylenimine) (PEI) have been explored. A dilatancy-based method is robocasting which makes use of a transition from pseudoplastic-to-dilatant behaviour.[13]

FDM requires accurate temperature control over very short time intervals. Colloid gel methods need careful control of the critical condition to change the ink from liquid to gel. Paste extrusion freeforming is relatively simple and requires no heating, cooling or cross-linking; the liquid-to-solid transition is realized by solvent evaporation. The paste preparation method is simple as well and many powders can be used with few changes to the formulation. Up to now, paste extrusion freeforming can

* Corresponding author. Tel.: +44 20 7679 4689.
E-mail address: j.r.g.evans@ucl.ac.uk (J.R.G. Evans).

0955-2219/$ – see front matter © 2009 Elsevier Ltd. All rights reserved.
doi:10.1016/j.jeurceramsoc.2009.07.019

Table 1
Typical materials for linear solid freeforming.

	Polymer or resin[2]	Colloid gel[3]	Sol–gel[14]	Paste[4]	High-solid-loading suspension[5]
Deposition material	ECG9/PZT	HA powder; disperant: Darvan 821A; dispersant: ammonium polyacrylate; binder: hydroxypropyl methylcellulose; antifoam agent: 1-octanol; gelling agent: poly(ethylenimine)	Polyvinyl-pyrrolidone (PVP); titanium diisopropoxide; bis(acetylacetonate) (TIA); solvent: propanol-2, ethanol, H_2O; agent: NH_4OH	PNZT powder; low-volatility solvent: α-terpineol; deflocculant: polyenoic acid, phosphate ester, fatty acid, fatty acid ester; binder: ethyl cellulose with a 48–49.5% ethoxy content	Mullite powder; disperant: Darvan 811; Na-PAA
Solid loading		45–50 vol.%		35%	60%
Viscosity, η	$\eta(T, \dot{\gamma}) = \eta(\dot{\gamma}) \cdot H(T)$; $H(T) = 1$–43 (383–413 K)	3 Pa s before gelation	Optimal range: 2.1–4.2 Pa s	50 Pa s	0.2–1 Pa s (pH 7.4)
Elasicity (G')		6×10^4 Pa	10^3–10^4 Pa		
Requirement of fabrication		Deposited under a non-wetting oil to prevent non-uniform drying	Air-powered fluid dispenser; pressure from 275 to 550 kPa; printing speed: 1600 μm/s	Time limit: 180–300 s	
Solidification	Cooling	Drain the oil and dry uniformly in air		Dry at 110 °C under vacuum	Sinter within 24 h of fabrication
Feature	It can feed material continuously	It can easily mix different inks before gelation		Extended paste ageing	Na^+ is introduced into the deposition material

deposit filaments with diameter of 80 μm and above[9] and is suitable for mass production.

The feed materials are very important for successful fabrication of structures, e.g. resin or polymer for FDM,[2] paste for EFF[1] and MP,[4] gel for DW[3] and high-solids-loading suspension for robocasting.[5] They should have rheological and solidification behaviour that enables flow through a fine nozzle under high shear and relatively low pressure.[13] Once the filament has been deposited, it should be rigid enough to maintain its shape and sustain a span. The filaments in lower layers must, of course, support those in the upper layers. Typical feed materials are listed in Table 1.

In this work, we used polyvinyl butyral polymer, itself often used as an adhesive in toughened glass, as the main binder.[16] It has high adhesion and damping properties and combines surface wetting properties with high cohesive strength. Thus, the paste transition from liquid to solid is realized with the aid of polymer transition from liquid to gel through solvent evaporation accompanied by an overall increase in solids content. We therefore investigate the characteristics of the paste during solvent evaporation around the liquid–solid transition because this is the critical stage in the fabrication process.[17] In order to quicken solidification, a relatively high volatility solvent, propan-2-ol was chosen. Finally, aperiodic woodpile photonic crystals and other structures were fabricated using different pastes.

2. Experimental details

2.1. Materials

The physical properties of the materials are listed in Table 2. The thermoplastic polymer, PVB and polyethylene glycol (PEG)

Table 2
The physical properties of materials used in this work.

Powder	Particle size (μm)	Type	Company
Al_2O_3	0.48	Purity: 99.992%	ex Condea Vista, Tucson Arizona, USA
Quartz	2	99.5%	PI-KEM Ltd., UK
$La(Mg_{0.5}, Ti_{0.5})O_3$ (LMT)	1		Prepared as in Ref. 8
Graphite	2	GS6E	GrafTech International Ltd., UK
Poly(vinyl butyral) (PVB)	–	BN18	Whacker Chemicals, UK
Poly(ethylene glycol) (PEG)	–	MWt = 600	VWR, UK
Propanol-2	–	GPR	VWR, UK

Table 3
Compositions of pastes expressed as volume fraction of solvent, V_s. The remaining components occupy $1 - V_s$ and are either polymer blend (column 2) or polymer blend and ceramic powder (columns 3–6) with a fixed volume fraction of powder, 0.6, based on the polymer–ceramic binary.

Materials	Polymer blend	Alumina	LMT	Quartz	Graphite
Solvent volume fraction	0.82 ± 0.07	0.49 ± 0.06	0.63 ± 0.17	0.61 ± 0.03	0.78 ± 0.06
	0.69 ± 0.02	0.46 ± 0.06	0.55 ± 0.07	0.59 ± 0.06	0.76 ± 0.09
	0.65 ± 0.02	0.37 ± 0.04	0.44 ± 0.07	0.55 ± 0.02	0.73 ± 0.06
	0.55 ± 0.01	0.29 ± 0.02	0.41 ± 0.03	0.50 ± 0.03	0.71 ± 0.01
	0.48 ± 0.02		0.37 ± 0.04	0.46 ± 0.01	
				0.39 ± 0.05	
				0.34 ± 0.04	

were used as binder. The powders were added to the organic solution, including PVB, PEG and propan-2-ol, and then dispersed by ultrasonic probe (U200S, IKA Labortechnik, Stanfen Germany). The pastes were prepared by stirring the suspension manually. The fabricated lattice structure was dried in the ambient environment, normally for more than 4 h. Debinding and sintering were accomplished in one step in air. The heating program was: room temperature to 400 °C at 2 °C/min; 400 °C to sintering temperature at 5 °C/min. There was a dwell at 400 °C and at the sintering temperature for 60 min and the cooling rate was 20 °C/min.

The rheological behaviour was measured by shear rate-controlled sweep and shear stress-controlled oscillation using an AR 2000 advanced parallel plate rheometer (TA Instrument Co., New castle, DE, USA) and HAAKE cone-plate Reostress 150 (Thermo Fisher Scientific, Waltham, MA, USA) with a 2°, 35 mm diameter cone. For oscillation, the frequency was 1 Hz. The paste was aged 30 min before measurement. The solvent volume fraction, defined throughout as the volume of solvent based on total volume, was established by averaging the volume fractions before and after the rheological experiment. The solvent volume fractions of pastes and errors caused by drying are given in Table 3.

2.2. Extrusion freeforming

The extrusion equipment is shown in Fig. 1. There are four axes: X, Y, Z and extrusion. The stainless steel syringe is mounted on the Z-axis and the sample substrate is placed on the X–Y table. The metal syringe with internal diameter of 9 mm was installed with extrusion dies with nominal diameters 500 μm, 300 μm or 150 μm (Models 1450, 1430, 1715, respectively, sapphire waterjet cutting nozzle, Quick-OHM, Wuppertal, Germany). The conical entry with angle of 79° was designed to facilitate paste entry to the nozzle from the cylinder. The extrusion pressure was measured by a load cell (Flintec, Redditch, UK) which was mounted on the extrusion axis.

3. Results and discussion

3.1. Viscosity of pastes

The polymer–ceramic paste properties are strongly dependent on the amounts of polymer, ceramic and solvent in the formulation. Since the technique uses the polymer transition from liquid to gel by solvent evaporation, the critical transition condition should be discernable through studies of rheological

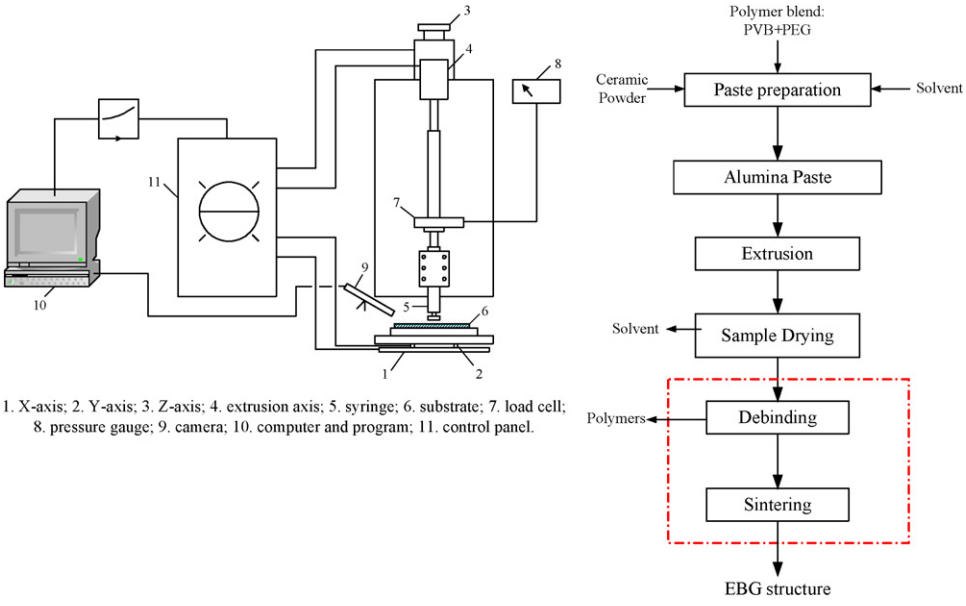

Fig. 1. Experimental set-up and process for extrusion freeforming showing three-axis table and two extruder drives.

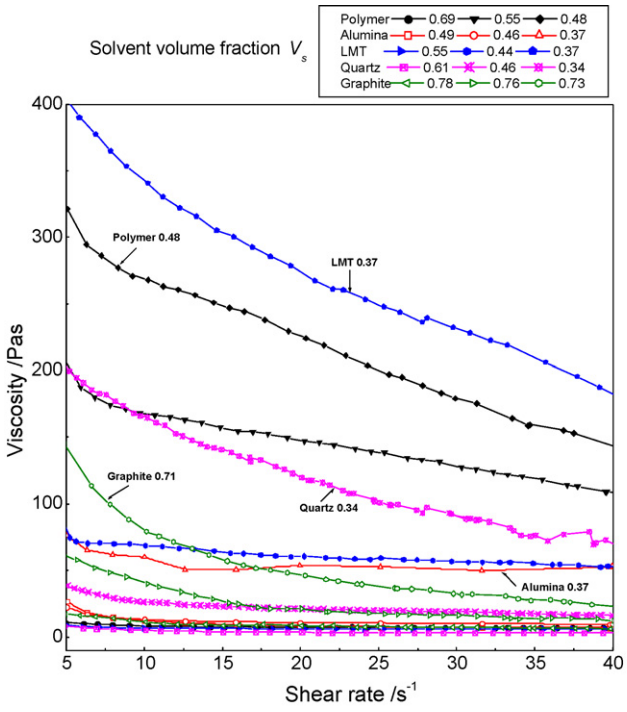

Fig. 2. Curves of viscosity vs. shear rate for pastes consisting of four different powders and polymer only.

properties. Initially, a paste based on the polymer constituents without ceramic powder was prepared, then alumina, LMT, quartz and graphite pastes (Table 3) were investigated. The powder-containing pastes all had 60 vol.% solids based on the polymer; the solvent content was varied systematically. The experimental results in Fig. 2 where solvent volume fraction is designated V_s, show that the shear rate dependence of viscosity as well as the absolute value of viscosity are influenced both by solvent content and the powder type. At higher solvent volume fractions, the viscosity is reasonably stable with increasing shear rate and the system approaches Newtonian behaviour. At lower solvent fraction, the viscosity decreases with increasing shear rate and these pastes behave as shear-thinning fluids showing pseudoplasticity.

The viscosity increases rapidly as the solvent content decreases for all these pastes, reaching a critical value that

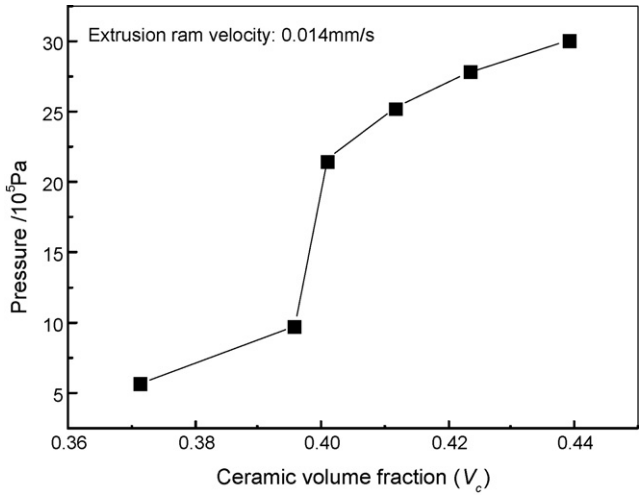

Fig. 4. Extrusion pressures recorded during steady state extrusion for alumina pastes with different solvent fractions.

indicates the effective state change. Fig. 3(a) shows how the viscosities of the different pastes change with overall ceramic volume fraction (based on the ceramic + polymer + solvent system) at a shear rate of 30 s^{-1}. There are transitional ceramic volume fractions for different pastes, below which the viscosity maintains a low value. If a small amount of solvent is lost by evaporation, the ceramic fraction rises beyond the transition point and viscosity rises dramatically. During paste extrusion, this tendency is reflected in the extrusion pressure. This was demonstrated for the alumina paste; the extrusion pressure was recorded as the ceramic volume fraction was varied using a ram velocity of 0.014 mm/s and a 0.5 mm diameter nozzle. The experimental results are shown in Fig. 4 from which it can be seen that there is a steep change when the ceramic fraction changes at 40 vol.%. The viscosity changed abruptly at this point also; Fig. 3(a) gives the ceramic volume fraction transition point for alumina paste close to 40%. The slight difference in transition point as evidenced by direct measurement of viscosity (Fig. 3(a)) and by extrusion pressure (Fig. 4) arises because the extrusion pressure is also influenced by other factors: backflow, friction and pressure drop in the paste, the last of these being influenced by plunger position. Viscosity measurement

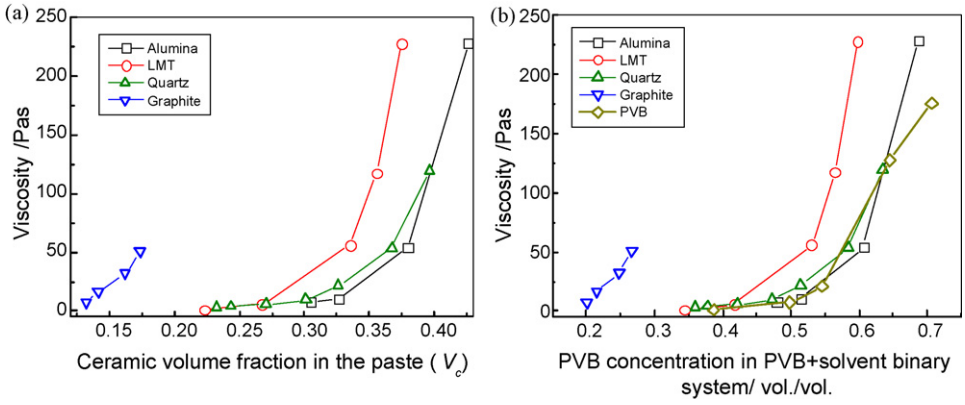

Fig. 3. Curves of viscosity as a function of (a) ceramic volume fraction and (b) polymer volume fraction in solvent only (all at a shear rate of 30 s^{-1}).

is thus the more reliable indicator. This gives a good indication that the freeforming process should operate around this liquid–solid transition point for this powder; the ideal ceramic fraction being below the transitional point. This means the viscosity is very low and the paste is easily extruded but with rapid solvent evaporation, the paste is quickly changed to the gel state.

There are however some differences among these pastes. The obvious characteristic is the liquid-to-solid transition point, which for LMT powder is around 34%. But for silica powder, the transition point is around 39%. For graphite powder, the value is 17%.

In order to compare the polymer concentrations (based now on the polymer–solvent binary) of ceramic pastes with that of the polymers without powder, Fig. 3(a) was redrawn to give Fig. 3(b). It is found that the liquid-to-solid transitional polymer concentrations for quartz and alumina pastes are equivalent nearly to the polymer liquid-to-gel transitional point which is around 0.6. This indicates that these pastes are polymer concentration controlled pastes; their liquid-to-solid transition points rely on the polymer concentration. But for the LMT and graphite pastes, the transitional polymer concentrations in the solvent are below 0.6. These two pastes are particle interaction controlled pastes where viscosity is mainly influenced by solids content based on the polymer–powder binary. Essentially, this is an indicator that the solids volume fraction based on the polymer–ceramic system is much closer to the maximum packing fraction for LMT and graphite powders.[18,19]

3.2. Elastic modulus of pastes

Elastic modulus has been evaluated for solid-like gels and is characterized in the absence of an equilibrium modulus by G', which exhibits a pronounced plateau extending to times at least of the order of seconds.[12] Smay et al. classified gels as 'weak' and 'strong' according to the value of elastic modulus,[20] and then deduced the minimum ink elasticity required to assemble a given periodic structure.[21]

Fig. 5(a) shows how the elastic modulus varies with shear stress for each paste. The pastes prepared from different powders show different elastic modulus ranges. The pastes from silica and alumina powders have higher moduli of around 10 kPa (shear stress: 0–100 Pa), but the pastes from LMT and graphite powder have lower moduli of below 600 Pa (shear stress: 0–100 Pa). The elastic modulus is related to features of the powder and the interaction between particles and polymers. It increases with reduced solvent fraction. Fig. 5(b) and (c) shows that when the solvent fraction decreases, the elastic moduli of quartz and alumina pastes increase.

When the extruded filament spans more than a critical distance, the filament deforms and sagging results as shown in Fig. 6(a). This behaviour may prevent extrusion freeforming from fabricating the designed structure with high quality. There are two situations leading to sagging: filament bending under a shear stress but below the yield stress. This is mainly controlled by effective elastic modulus. Secondly, the filament may deform under a shear stress beyond the yield stress; this being determined by the value of yield stress and by creep behaviour. The

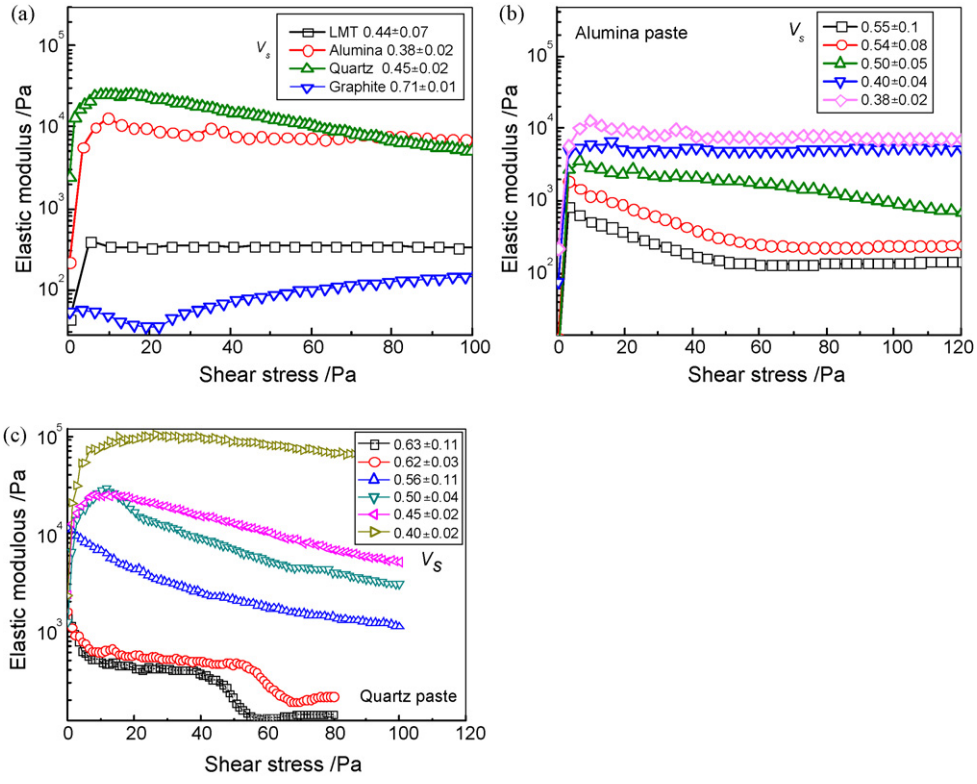

Fig. 5. Elastic modulus as a function of shear stress for (a) four different powders at solvent volume fractions suitable for the extrusion process, (b) alumina paste at different solvent contents and (c) quartz paste at different solvent contents (solvent volume fractions, V_s, are given).

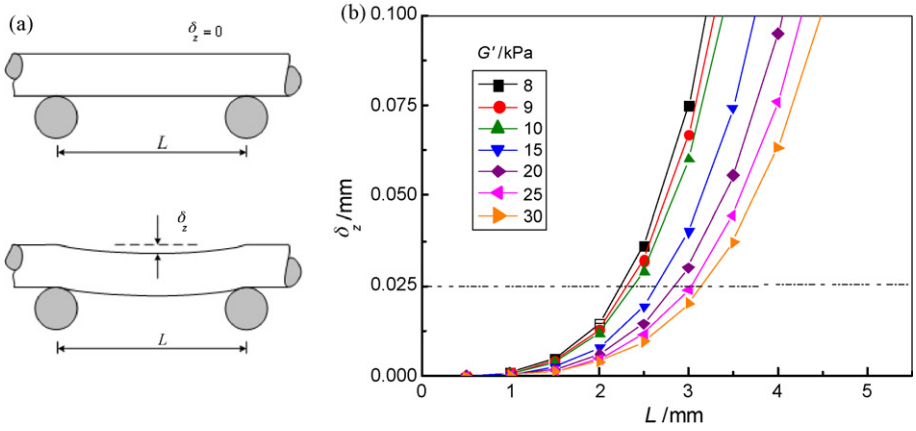

Fig. 6. Filament deformation: (a) schematic filament bending (deviation δ_z and span distance L); (b) relationship between maximum deviation ($\delta_{z\max}$) and span distance (L) for different elastic modulus if the paste (G') (dashed line represents a tolerance 5%).

extrusion conditions could also affect deformation, for example through polymer orientation effects but these should relax quickly. Thus when below the liquid-to-solid transition, the paste viscosity does not change with time as shown in Fig. 7(a) or shear rate as shown in Fig. 2. However, when beyond the transitional point, relaxation processes could be considerably extended. The first mechanism, elastic deformation, is generally thought to operate. Smay et al.[21] deduced an effective Eq. (1) to estimate filament deviation. In order to evaluate the sagging, a simply supported beam is considered on the basis that the weld remains deformable in the early stages of drying. As shown in Fig. 6(a), the distance between the filament centre and the horizontal can be calculated by the following equation[21]:

$$\delta_z = \frac{Wy}{24EI}(2Ly^2 - y^3 - L^3) \tag{1}$$

where W is the distributed load, y the position along the rod, E the Young's modulus of the paste and I the area moment of inertia of the circular cross section. Inserting the values for alumina paste:

$$W = 0.25\rho_{paste} g\pi D^2 \tag{2}$$

where D is filament diameter, 0.5 mm; ρ_{paste} is paste density 2182 kg m^{-3} when solvent content is 37%.

$$E = (1 + \nu)2G' \tag{3}$$

where ν is Poisson's ratio for the filament, typically $\nu = 0.25$ according to Ref. 22; and G' is elastic modulus of the paste.

$$I = \frac{\pi D^4}{64} \tag{4}$$

As $y = L/2$, δ_z reaches the maximum value $\delta_{z\max}$, for the filament deformation.

Relying on Eqs. (2)–(4), Eq. (1) becomes

$$\delta_{z\ \max} = \frac{2.4041L^4\rho_{paste}}{2.9438D^2G'} \tag{5}$$

Eq. (5) shows the relationship between $\delta_{z\max}$ and L under different G'. Based on Eq. (5), Fig. 6(b) gives the curves of $\delta_{z\max}$ versus L for different values of G' when $D = 0.5$ mm and $\rho_{paste} = 2182$ kg m^{-3} for the maximum allowable deviation which is 5% of diameter:

$$\delta_{z\ \max} = \frac{D}{20} \tag{6}$$

This specification was selected because it did not produce significant errors in bandgap frequency in millimeter wave bandgap structures.[23]

So the intersection of the $\delta_{z\max}$–L curve and the line representing the maximum allowable deviation is the maximum allowable span distance for different values of elastic modulus

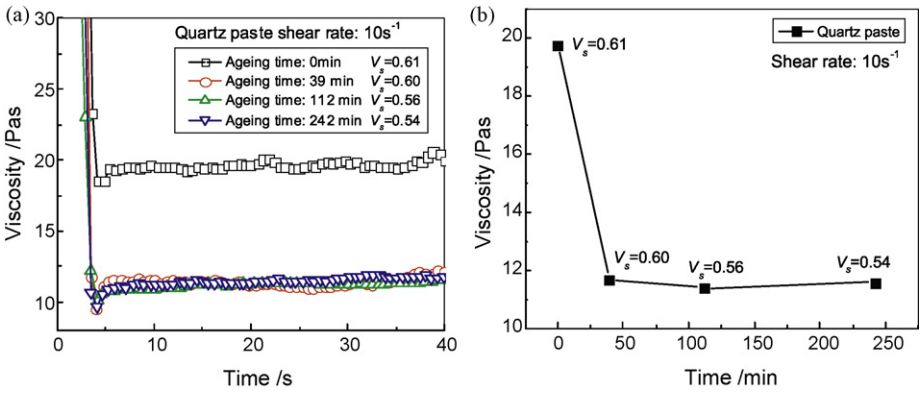

Fig. 7. The approach to steady state viscosity recorded on pastes which had been aged for different times.

of the paste. From Fig. 5(b), the alumina paste elastic modulus is around 10 kPa at a solvent content of 37%. Transferring to Fig. 6(b), it can be deduced that the maximum allowable span is about 2 mm. Thus design tolerance specification can be assessed directly from paste rheology.

3.3. Paste ageing

Ageing phenomena in pastes prepared from untreated powders can involve the time-dependence of adsorption reactions of surface active agents, the diffusion of solvents, particularly volatile solvents which result in spatial inhomogeneity during mixing, rheological recovery in thixotropic pastes and relaxation of steric constraints between interlocking particles.[24] Solvent fraction, stirring history and particle characteristics can influence ageing behaviour. In this case, redistribution of solvent and hence homogenising the composition is the main aim.

Morissette et al. studied the effect of ageing on paste properties using α-Terpineol as a low-volatility solvent[4] showing that pastes prepared from as-received powders attained printable viscosity after 50 days (4.3 Ms) of ageing and paste prepared from dispersant-coated powders needed 1 day (86 ks) of ageing. In order to investigate the effect of solvent redistribution by ageing on paste rheological properties, the quartz paste was tested under constant shear rate. The aging period is recorded from the moment when paste stirring stopped and the sample was placed in a sealed container, this time-point is designated 0 min in Fig. 7. The rheological experiment was performed within 3 min of removing the sample from the container. Solvent contents were recorded before and after viscosity measurement. At ageing time-points of 39 min (2.34 ks), 112 min (6.72 ks) and 242 min (14.52 ks), the viscosities were measured at a shear rate of 10 s^{-1} and the results are recorded in Fig. 7. After aging the paste for 39 min, viscosity decreased from 19 Pa s to 11 Pa s. Prolonging the time did not produce a further effect. So in this experiment, the proponal-2 based PVB paste needs to be aged for only about 30 min before fabrication can begin.

The viscosity (11 Pa s, m_s: 0.34) obtained from this experiment with constant shear rate (10 s^{-1}) in Fig. 7 is close to that (8 Pa s (10 s^{-1}), m_s: 0.35) from the experiment with increasing shear rate in Fig. 2(d) with a slightly higher solvent content.

3.4. Fabrication of structures

In order to demonstrate paste extrusion fabrication using these pastes, we first built aperiodic EBG structures with alumina (dielectric constant: $\varepsilon_r = 9.6$ (100 GHz)) designed to have four layers in which the first and third layers have inter-filament distances (defined as the separation of adjacent filament centre lines) steadily increasing from 0.4 to 1.58 mm along the edge to the middle of the structure. This aperiodic structure is shown in Fig. 8(a). In the second and fourth layers, the distance between filaments is constant with $a = 1.6$, $w = 0.4$ (where a is the distance between two filament centres and w the filament width). In the first and third layers, the designed distances between successive filaments are shown in Fig. 8(b). These aperiodic structure designs are helpful for estimating the maximum permitted freedom in local disorder. They can also be used to test the construction principle for variable size photonic bandgap structures, which are applicable for beam-shaping devices as

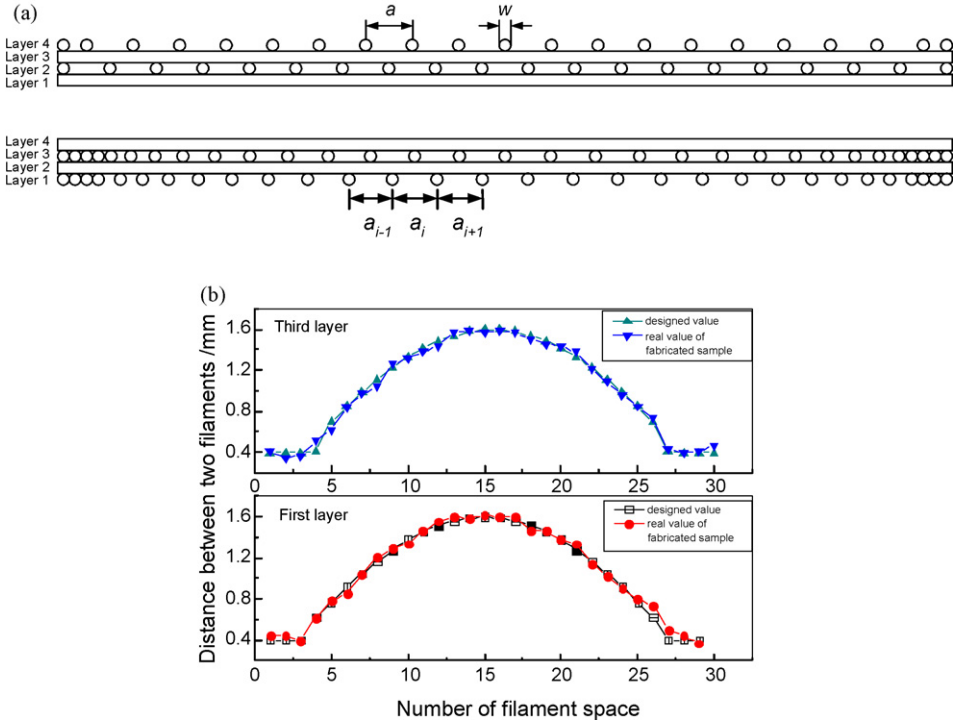

Fig. 8. Dimension of aperiodic EBG structure (a) side elevation of the aperiodic EBG structure; (b) design value and fabricated values of structure for successive filament distances.

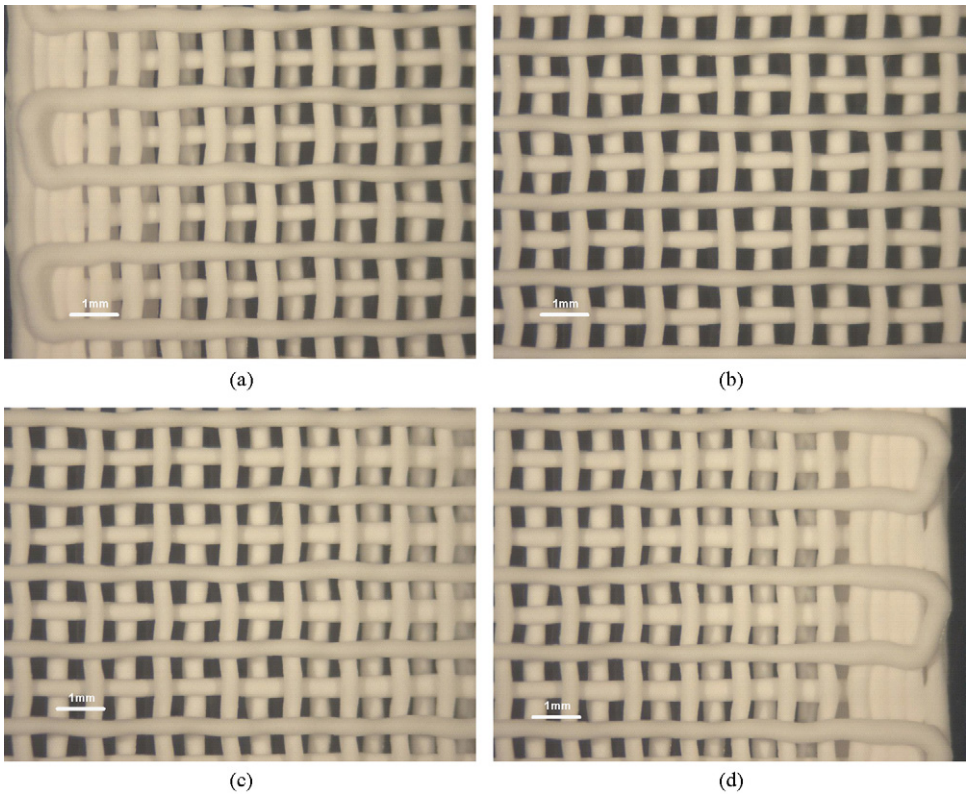

Fig. 9. Images of the top view of a sintered aperiodic EBG structure by optical microscopy.

well as for other applications such as arbitrary angle waveguides or modified convex superprism devices.[25] From a construction point of view, the aperiodic structure provides a good test for deformation of the filament between supporting members.

During fabrication, the ram extrusion velocity was 0.014 mm/s, the XY table velocity was 3.8 mm/s, and the recorded pressure was close to 15 MPa. The dimensions are $a = 2.0$ mm, $w = 0.5$ mm. The final component, after drying, pyrolysis and sintering, is shown in Fig. 9 from which it can be seen that in the fourth layer, filament bending is not detected when the filaments span the distances from 0 to 1.96 mm. In the third layer, the filaments span constant distances of 2 mm, but the filament deforms downwards in some regions. The reason for this is that the filament has to bear the filament weight in the upper layer as well as its own weight. It indicates that the maximum allowable span distance for this deposition material is 2 mm when the 0.5 mm diameter nozzle is used.

The sintered filament diameters and distances between two filament centres were measured with an optical microscope (Meiji Binocular, Saitama, Japan). The shrinkage was obtained by $(a_d - a_s)/a_d$, where a_d, fabricated distance between two filament centres; a_s, sintered distance between two filament centres. The shrinkage of the first layer and the third layer were 0.18 ± 0.06 and 0.19 ± 0.05, respectively. The shrinkage ratio for the second layer and the fourth layer were 0.19 ± 0.02. The overall average shrinkage ratio is 0.19. The fabricated aperiodic distances between successive filaments are shown in Fig. 8(b). The filament diameter (w) is 0.38 ± 0.04 mm. The periodic distance (a) between two filaments in the second and fourth layer is 1.62 ± 0.05 mm. This gives an indication of the fabrication accuracy.

The transmission characteristic of the electromagnetic crystals was measured using the Gaussian beam free space measurement system.[26] The attenuation of the transmission amplitude as a function of frequency through the fabricated aperiodic woodpile EBG crystal is shown in Fig. 10. It demonstrates that a large and sharp bandgap is exhibited in the frequency region of 100–110 GHz. In order to compare this spectrum with the bandgap of a four-layer periodic woodpile structure which we fabricated based on the dimensions $w = 0.4$ mm, $a = 1.6$ mm,

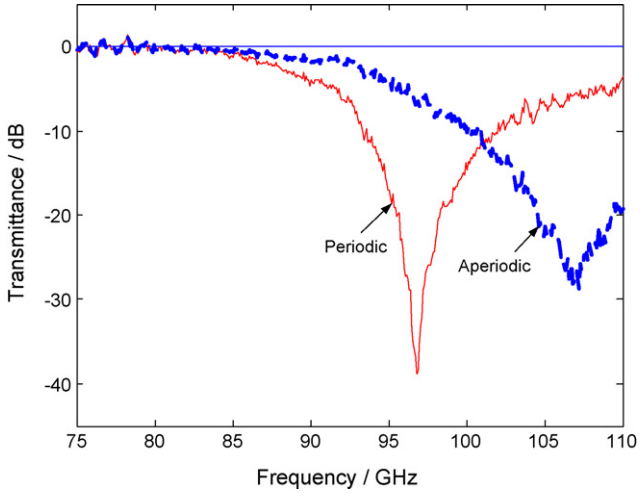

Fig. 10. Transmittances of EBG woodpile structures as a function of frequency.

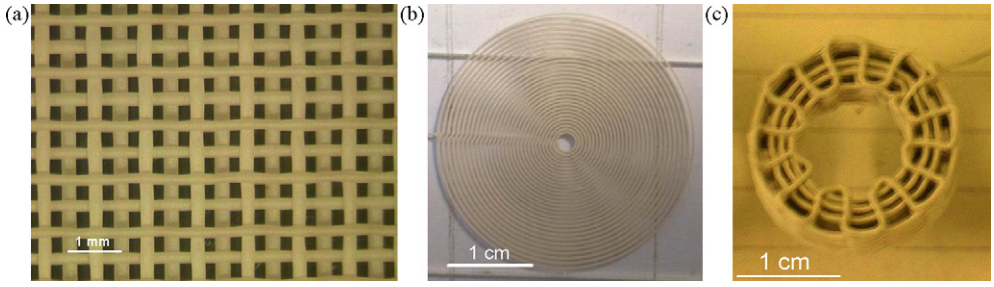

Fig. 11. Structures fabricated by extrusion freeforming: (a) periodic woodpile structure (4 layers) fabricated with LMT paste; (b) circle ring structure (2 layers) fabricated with quartz paste; (c) cylindrical structure (8 layers) with alumina paste.

its transmission is also plotted in Fig. 11 and its bandgap is in the 90–100 GHz region. The maximum attained attenuations for periodic woodpile and aperiodic woodpile structures are −39 dB at 97 GHz and −29 dB at 107 GHz, respectively. This proves that the aperiodic woodpile structure can also generate a bandgap. The experimental results indicate that a ceramic paste with high volatility solvent can be used for fabrication of lattice EBG structures by extrusion freeforming.

In addition to aperiodic EBG structures, we fabricated similar structures using LMT paste using a 300 μm nozzle, a circular ring structure with one layer sitting on another layer using quartz paste through a 150 μm nozzle (radius of outer ring: 15.05 mm; radius of inner ring: 1.27 mm) and a cylindrical structure with alumina paste through a 500 μm nozzle (radius of outer ring: 10.00 mm; radius of inner ring: 6.00 mm), as shown in Fig. 11. Various ceramic lattices designed for hard tissue scaffolds are shown in Ref.27. These structures demonstrate that solvent-based paste extrusion freeforming is suitable for widely different powders and different patterns.

4. Conclusions

Solvent-based paste extrusion freeforming can be used for fabrication of tissue scaffolds and photonic crystals. The characteristics of the paste define the design tolerance. In this paper, different pastes prepared from alumina, quartz, LMT, graphite and polymer only were investigated under diverse conditions including different solvent fractions and ageing times. The principle for this technique is transition of the paste from liquid to solid by solvent evaporation. The experimental results showed that the pastes can be designated: polymer controlled where viscosity increase at reducing solvent contents follows the curve for the polymer solution or particle interaction controlled where viscosity is mainly influenced by solids content. Thus the polymer-controlled pastes behave rheologically just as the polymer, reaching a transition point at the same solvent content at which the polymer solution changes from liquid to gel. For the particle interaction controlled paste, the transition is lower than that of polymer. As the solvent fraction decreases, the viscosity and elastic modulus rise. Modulus obtained from rheological measurement can be used to define the specifications for filament deformation in the structure. The paste needs to be aged before fabrication. Finally, structures were fabricated which demonstrate the capability of this technique and its versatility in terms of deployment of diverse powders.

Acknowledgements

The authors gratefully acknowledge the financial support from the Leverhulme Trust (Grant No. F/07476/V).

References

1. Grida, I. and Evans, J. R. G., Extrusion freeforming of ceramics through fine nozzles. *J. Eur. Ceram. Soc.*, 2003, **23**, 629–635.
2. Bellini, A., Shor, L. and Guceri, S. I., New developments in fused deposition modelling of ceramics. *Rapid Prototyp. J.*, 2005, **11**(4), 214–220.
3. Michna, S., Wu, W. and Lewis, J. A., Concentrated hydroxyapatite inks for direct-write assembly of 3-D periodic scaffolds. *Biomaterials*, 2005, **26**, 5632–5639.
4. Morissette, S. L., Lewis, J. A., Clem, P. G., Cesarano, J. and Dimos, D. B., Direct-write fabrication of Pb (Nb, Zr, Ti)O_3 devices: influence of paste rheology on print morphology and component properties. *J. Am. Ceram. Soc.*, 2001, **84**(11), 2462–2468.
5. Stuecker, J. N., Cesarano, J. and Hirschfield, D. A., Control of the viscous behaviour of highly concentrated mullite suspensions for robocasting. *J. Mater. Process. Technol.*, 2003, **142**, 318–325.
6. Lewis, J. A. and Gratson, G. M., Direct writing in three dimensions. *Mater. Today*, 2004, **7**, 32–39.
7. Gratson, G. M., Garcia-Santamaria, F., Lousse, V., Xu, M., Fan, S., Lewis, J. A. and Braun, P. V., Direct-write assembly of three-dimensional photonic crystals: conversion of polymer scaffolds to silicon hollow-woodpile structures. *Adv. Mater.*, 2006, **18**, 461–465.
8. Lu, X., Lee, Y., Yang, S., Hao, Y., Ubic, R., Evans, J. R. G. and Parini, C. G., Fabrication of electromangtic crystals by extrusion freeforming. *J. Am. Ceram. Soc.*, 2009, **92**(2), 371–378.
9. Yang, H., Yang, S., Chi, X. and Evans, J. R. G., Fine ceramic lattices prepared by extrusion freeforming. *J. Biomed. Mater. Res. B: Appl. Biomater.*, 2006, **79**, 116–121.
10. Wang, T. M., Xi, J. T. and Jin, Y., A model research for prototype warp deformation in the FDM process. *Int. J. Adv. Manuf. Technol.*, 2007, **33**, 1087–1096.
11. Tellis, B. C., Szivek, J. A., Bliss, C. L., Margolis, D. S., Vaidyanathan, R. K. and Calvert, P., Trabecular scaffolds created using micro CT guided fused deposition modeling. *Mater. Sci. Eng. C*, 2008, **28**, 171–178.
12. Almdal, K., Dyre, J. and Hvidt, S., Towards a phenomenological definition of the Term "Gel". *Polym. Gels Networks*, 1993, **1**, 5–17.
13. Lewis, J. A., Smay, J. E., Stuecker, J. and Cesarano, J., Direct ink writing of three-dimensional ceramic structures. *J. Am. Ceram. Soc.*, 2006, **89**(12), 3599–3609.
14. Duoss, E. B., Twardowski, M. and Lewis, J. A., Sol–gel inks for direct-write assembly of functional oxides. *Adv. Mater.*, 2007, **19**, 3485–3489.
15. Gratson, G. M., Xu, M. and Lewis, J. A., Microperiodic structures: direct writing of three dimensional webs. *Nature*, 2004, **428**, 386.

16. Lu, X., Lee, Y., Yang, S., Hao, Y., Ubic, R., Evans, J. R. G. and Parini, C. G., Fabrication of electromagnetic crystals by extrusion freeforming. *Metamaterials*, 2008, **2**, 36–44.
17. Winter, H. H. and Mours, M., Rheology of polymers near liquid–solid transitions. *Adv. Polym. Sci.*, 1997, **134**, 165–234.
18. Chong, J. S., Christiansen, E. B. and Baer, A. D., Rheology of concentrated suspensions. *J. Appl. Polym. Sci.*, 1971, **15**, 2007–2021.
19. Zhang, T. and Evans, J. R. G., Predicting the viscosity of ceramic injection moulding suspensions. *J. Eur. Ceram. Soc.*, 1989, **5**(3), 165–172.
20. Smay, J. E., Gratson, G. M., Shepherd, R. F., Cesarano III, J. and Lewis, J. A., Directed colloidal assembly of 3D periodic structures. *Adv. Mater.*, 2002, **14**, 1279–1283.
21. Smay, J. E., Cesarano III, J. and Lewis, J. A., Colloidal inks for directed assembly of 3-D periodic structures. *Langmuir*, 2002, **18**, 5429– 5437.
22. Tilbrook, M. T., Moon, R. J. and Hoffman, M., On the mechanical properties of alumina-epoxy composites with an interpenetrating network structure. *Mater. Sci. Eng. A*, 2005, **393**, 170–178.
23. Lu, X., Lee, Y., Yang, S., Hao, Y., Ubic, R., Evans, J. R. G. and Parini, C. G., Fabrication and evaluation of solid freeformed electromagnetic bandgap structures. *J. Phys. D: Appl. Phys.*, 2009, **42**, 145107.
24. Cloitre, M., Borrega, R. and Leibler, L., Rheological aging and rejuvenation in microgel pastes. *Phys. Rev. Lett.*, 2000, **85**, 4819–4822.
25. Zarbakhsh, J., Mohtashami, A. and Hingerl, K., Geometrical freedom for constructing variable size photonic bandgap structures. *Opt. Quantum Electron.*, 2007, **39**(4–6), 395–405.
26. Lee, Y., Lu, X., Hao, Y., Yang, S., Ubic, R., Evans, J. R. G. and Parini, C. G., Rapid prototyping of millimetrewave metamaterials: simulations and experiments. *Microwave Opt. Technol. Lett.*, 2007, **49**(9), 2090–2093.
27. Yang, S., Yang, H., Chi, X., Evans, J. R. G., Thompson, I., Cook, R. J. and Robinson, P., Rapid prototyping of ceramic lattices for hard tissue scaffolds. *Mater. Des.*, 2008, **29**(9), 1802–1809.